SURFACE AND INTERFACE ANALYSIS
Surf. Interface Anal. **30**, 444–447 (2000)

Scanning Hall probe microscopy observation of flux pinning in a Pb film covering an array of Co dots

J. Bekaert,[1]* M. J. Van Bael,[1] K. Temst,[1] L. Van Look,[1] V. V. Moshchalkov,[1] Y. Bruynseraede,[1] G. D. Howells,[2] A. N. Grigorenko,[2] S. J. Bending[2] and G. Borghs[3]

[1] Laboratorium voor Vaste-Stoffysica en Magnetisme, Katholieke Universiteit Leuven, Celestijnenlaan 200D, B-3001 Leuven, Belgium

[2] Department of Physics, University of Bath, Claverton Down, Bath BA2 7AY, UK

[3] Interuniversity Micro-electronics Center (IMEC vzw), Kapeldreef 75, B-3001 Leuven, Belgium

High-resolution scanning Hall probe microscopy (SHPM) has been used to investigate the superconducting properties of a thin Pb film covering a square array of rectangular submicron Co dots. After magnetization, all the dots are shown to be in a single-domain magnetic state with dipole stray field distributions. As the sample is cooled through the critical temperature of the Pb film at $B = 0$ we observe strong screening of the dipole fields that we attribute to fluxoid quantization in the superconducting state. Upon cooling in applied perpendicular fields we show that the first flux line is selectively pinned at the pole of the magnet with the opposite sign of stray field. Ordered vortex structures, which are commensurate with the underlying pinning array, are observed at fields up to twice the matching field. At fields in excess of the first matching field, each pinning site appears to be capable of trapping at least two flux lines and no evidence is seen for interstitial vortices up to twice the matching field at temperatures well below the critical temperature of the covering Pb film.

KEYWORDS: magnetic field mapping; Hall sensor; flux pinning

INTRODUCTION

Over the last decade, advances in microfabrication have allowed the production of superconducting samples with ordered artificial pinning arrays, e.g. an antidot lattice in a thin film.[1–3] These artificial pinning arrays give rise to a strong enhancement of the bulk magnetization (M) and critical current (j_c) and have been used successfully to gain insight into the microscopic nature of pinning. Commensurability effects between the periodic vortex lattice and ordered pinning arrays with various symmetries have also been studied and stable vortex configurations have been imaged directly using Lorentz microscopy.[4] The integrated response from a large number (typically 10^6) of vortices corresponding to these configurations has been investigated by magnetization and critical current measurements.[1–3] More recently, regular arrays of ferromagnetic dots have been explored where, besides the core pinning, additional contributions arise due to the interaction of the vortices with the local magnetic fields generated by the dots.[5–8] Although macroscopic commensurability effects have already been demonstrated in such systems, insight into the microscopic origin of these flux line structures is still lacking. The system studied here is a type II superconducting Pb film deposited on top of an ordered lattice of magnetic dipoles consisting of single-domain Co dots with in-plane magnetization. Using scanning Hall probe microscopy (SHPM) we directly visualize the vortex configurations simultaneously with the local stray fields of the magnetic pinning centres. Our experiments show that the flux lines are preferentially pinned at that side of the dipole where the stray field is opposite to that of the flux line, and hence give a direct indication of the microscopic interaction mechanism of flux lines with the local stray field of magnetic pinning centres. At fields above the first matching field, multi-quanta vortex lattices are visualized.

SAMPLE DESCRIPTION

Square lattices (period $a = 1.5$ μm) of rectangular submicron polycrystalline magnetic dots, consisting of a Au (7.5 nm)/Co (20 nm)/Au (7.5 nm) trilayer on a SiO_2 substrate, are fabricated by electron beam lithography and molecular beam deposition. The dots have lateral dimensions of 540 nm (easy axis) × 360 nm. Magnetic force microscopy (MFM) measurements at room temperature reveal a multi-domain structure in the as-grown state. After magnetization along the easy axis, all dots are in

* Correspondence to: J. Bekaert, Laboratorium voor Vaste-Stoffysica en Magnetisme, Katholieke Universiteit Leuven, Celestijnenlaan 200D, B-3001 Leuven, Belgium.
E-mail: joost.bekaert@fys.kuleuven.ac.be

Contract/grant sponsor: Fund for Scientific Research, Flanders (FWO).
Contract/grant sponsor: Belgian IUAP.
Contract/grant sponsor: Flemish GOA.
Contract/grant sponsor: British EPSRC.
Contract/grant sponsor: British MOD; Contract/grant number: GR/J03077.
Contract/grant sponsor: University of Bath.

Received 15 July 1999
Revised 3 December 1999; Accepted 3 December 1999

a stable remanent single-domain state. The lattice of Co dots was covered with a 50 nm superconducting Pb film, a protective Ge layer (20 nm) and a 10 nm Au layer for the scanning tunnelling microscopy (STM) distance control of the SHPM. Further details on the sample fabrication and characterization are presented elsewhere.[7]

SCANNING HALL PROBE MICROSCOPY SET-UP

The SHPM set-up used is a modified commercial low-temperature scanning tunnelling microscope where the tunnelling tip is replaced by a GaAs/AlGaAs heterostructure chip. A Hall probe was defined in a two-dimensional electron gas at the intersection of two 200 nm wide wires $\sim$5 μm from the corner of a deep mesa etch. The latter had been coated with a thin Au layer to act as an integrated STM tip allowing the simultaneous measurement of local magnetic induction and surface topography. In practice the sample is first approached towards the sensor using an inertial coarse approach mechanism until tunnelling is established and then retracted $\sim$100 nm, allowing rapid scanning with little risk of damaging the Hall sensor. The Hall probe is mounted at an angle of $1-2^\circ$ with respect to the sample plane to ensure that the STM tip is always the closest point to the surface. We estimate that the active Hall sensor was $\sim$200–300 nm above the sample during the scans shown here. A more detailed description of SHPM can be found elsewhere.[9,10]

RESULTS AND DISCUSSION

In what follows, we describe measurements at temperatures above and below the superconducting critical temperature of the Pb film ($T_c = 7.16$ K) with an applied field normal to the sample plane. The first matching field B_1 is defined as the field at which exactly one flux quantum ϕ_0 is present per unit cell of the pinning array, i.e. $B_1 \equiv \phi_0/a^2 = 9.2$ G.

Figure 1 shows an SHPM image of a region near the centre of the sample at $B = 0$ and $T = 7.3$ K. The scanned surface region is 6 μm × 6 μm. Prior to this and all further measurements, the sample was magnetized along the easy axis of the dots in a field of 0.5 T. At this temperature the Pb film is in the normal state and the dipole stray fields characteristic of an ordered array of single domain particles can be seen clearly.

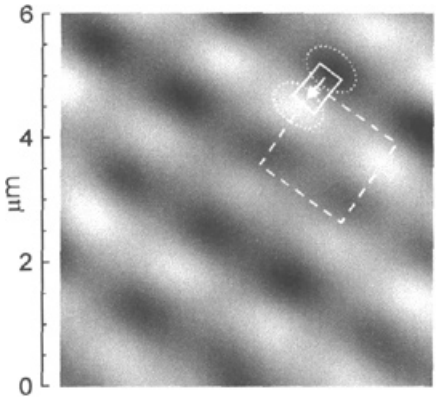

Figure 1. The SHPM image of a square lattice of single-domain Co dots at 7.3 K. The grey scale represents the magnitude of the perpendicular component of the local stray field b (bright: $b > 0$, dark: $b < 0$). Here, the total grey scale is 4.2 G. As a guide to the eye, the unit cell of the dot array, the position of one dot and a magnetization vector are also indicated.

As the sample is cooled down through the critical temperature of the Pb film at $B = 0$ we see a pronounced screening of the dipole fields in the superconducting state. The peak-to-valley induction modulation fields (i.e. the peak-to-peak difference between the maximal positive and negative local field) has been measured over an area of 3 μm × 3 μm with no applied external field as a function of temperature. In the superconducting state we see an increase of $\sim$0.35 G in this quantity, which far exceeds the noise level of our measurement system. Our interpretation of this observation is that screening currents are generated in the Pb film near the poles of the Co magnet in order to satisfy fluxoid quantization. In that case, the flux threading the Pb film above T_c at each pole would be slightly less than one flux quantum ϕ_0, which is a realistic estimate. We note also that, due to the relatively large sample–sensor spacing, many field lines will loop back on themselves underneath the Hall probe, resulting in a gross underestimate of the net measured flux.

The SHPM results at $B/B_1 = 1/2$ and $T = 6.5$ K $< T_c$ after field cooling are shown in Fig. 2. In order to identify

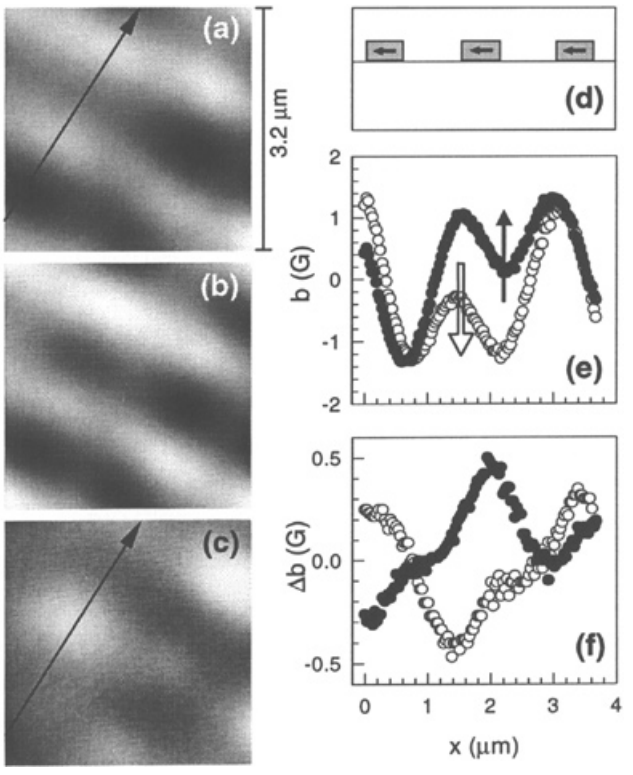

Figure 2. Scanning Hall probe microscopy images: (a) at $T = 6.5$ K $< T_c$ and $B/B_1 = 1/2$; (b) of the same sample area at $T > T_c$ and $B/B_1 = 1/2$; (c) image obtained after subtracting (b) from (a). (d) Schematic presentation of the dot positions along the arrows in (a) and (c). (e) Local field distribution at $T = 6.5$ K along the arrow direction in (a) at $B/B_1 = 1/2$ (filled symbols) and $B/B_1 = -1/2$ (open symbols); the black and white arrows indicate the suggested positions of the positive and negative flux line, respectively. (f) Field distribution along the same arrow as indicated in (c) after subtraction of the dipole contribution for $B/B_1 = 1/2$ (filled symbols) and $B/B_1 = -1/2$ (open symbols).

the vortex locations, we subtract the dipole contribution at $T > T_c$ [Fig. 2(b)] from the image at $T < T_c$ [Fig. 2(a)], which gives Fig. 2(c), containing information about the flux lines. The white spots in Fig. 2(c) are to be associated with the positive flux lines. A closer comparison of Figs 2(b) and 2(c) reveals that each flux line is positioned on a specific side of the dot, namely on this pole where the local stray field points in the opposite direction compared to that of the flux line. Figure 2(e) shows the measured total (i.e. of magnetic dots and flux lines) local field profile $b(x)$ at $B/B_1 = +1/2$ and $-1/2$ along the arrow direction in Fig. 2(a). The position of the dots along this arrow is indicated schematically in Fig. 2(d). For the dots only, one would expect a field signal that is oscillating around $b = 0$ with a constant amplitude due to the succession of positive and negative magnetic poles. In Fig. 2(e), it can be seen that due to the presence of a positive flux line ($B/B_1 = 1/2 > 0$, black symbols) the local field at the negative pole of the central dot is suppressed, whereas in the case of a negative flux line ($B/B_1 = -1/2 < 0$, open symbols) the positive pole is suppressed, indicating that a flux line is pinned at the opposite pole of the dipole. This pole selectivity can be understood because a free vortex and an antivortex, here formed by the opposite pole of the magnetic dot, will attract and ultimately annihilate one another. Figure 2(f) shows the same line scans as in Fig. 2(e), but this time the dipole signal from the dots is subtracted. These line scans clearly show that the pinning positions of the positive and the negative vortices are separated by $\sim$0.6 μm, which is very close to the dot length and indicates that vortices of different polarity are selectively pinned at the opposite ends of the nanomagnets. Contrary to the case of perpendicularly magnetized dots,[6] where it was found that the positive vortices are pinned at dots with moment pointing in the same positive direction due to the strong interaction of the flux line with the magnetic moment of the dots, the direct interaction of the (perpendicular) local vortex field with the magnetic moment of the dot is absent for dots with in-plane magnetization. In our experiment, we could therefore isolate the interaction of the flux line with the local stray field from the interaction with the magnetic moment of the dot. In a general case of flux pinning at a magnetic pinning centre, the dominant interaction mechanism is obtained by balancing all different interaction contributions.

Figure 3 shows SHPM images at field values $B/B_1 = 1/2$, 1, 3/2 and 2 after field cooling. In all cases, an ordered vortex structure is observed, which is commensurate with the underlying square pinning array. At $B/B_1 = 1/2$ [Fig. 3(a)] we observe the 'checkerboard' structure where every second dot is occupied by a flux line, forming a square vortex lattice rotated by 45° with respect to the pinning array. At B_1 [Fig. 3(b)] every dot traps a single flux line and the vortex structure mirrors that of the dot array. For $B/B_1 = 3/2$ [Fig. 3(c)] the structure is a direct superposition of that for $B/B_1 = 1/2$ and $B/B_1 = 1$, where half of the sites pin two flux quanta (these are the brighter spots with a higher local field value) and the rest trap just one. Finally for $B/B_1 = 2$ [Fig. 3(d)] every dot has trapped two flux lines, except for one dot in the bottom right corner that has three flux quanta associated with it, possibly due to a small sample inhomogeneity or because the applied field slightly exceeds $2B_1$. Figures 3(e)–3(h) show line scans along the indicated arrows, and confirm our vortex assignments. Figures 3(i)–3(l) schematically show the pinning of vortices (open circles) on the dot positions (black dots). Although the location of the first pinned vortex on a dot can be well resolved and established, it is not clear from an experimental or theoretical point of view where the flux lines carrying more than one flux quantum are attached to a dot. Up to $2B_1$ we see no evidence for vortices occupying interstitial positions at these low temperatures ($T \leq 6.5$ K). Earlier macroscopic $M(B)$ and $j_c(B)$ data on similar samples at temperatures very close to T_c have shown an abrupt drop at $B = B_1$, which was attributed to the presence of weakly pinned interstitial vortices.[1,11,12] We note that, due to the divergence of the

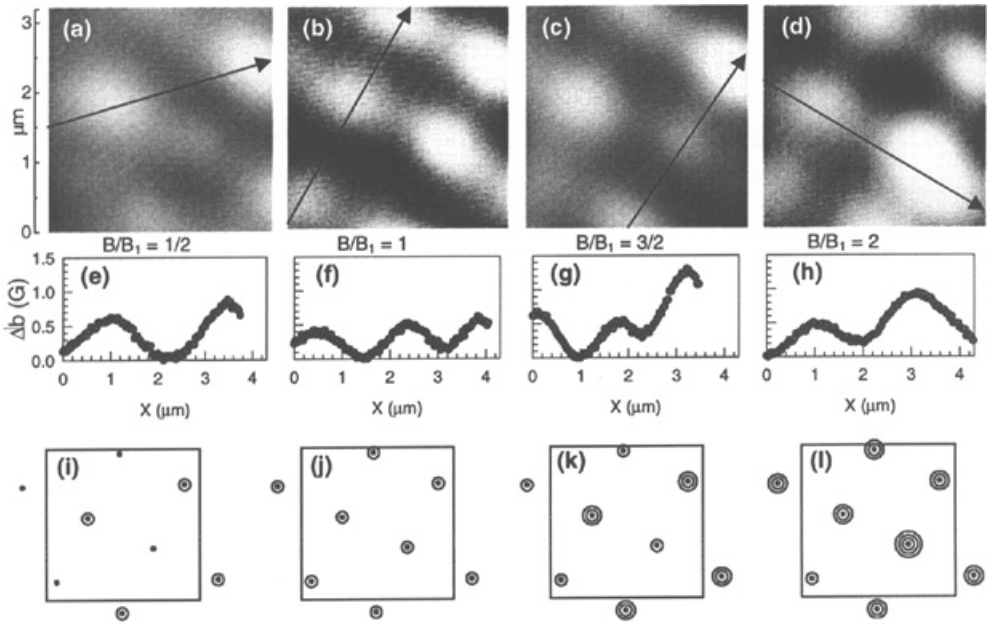

Figure 3. (a–d) Scanning Hall probe microscopy images at $T = 6.5$ K after subtraction of the dipole contribution at different values of B/B_1 as indicated. (e–h) The local field distribution along the arrow directions in (a), (b), (c) and (d), respectively. (i–l) Schematic representation of the dot array (points) and configuration of pinned vortices (circles) for the different B/B_1 values.

penetration depth $\lambda(T)$ at T_c, a very different behaviour can indeed be expected in such different temperature regimes. The results in this paper are only valid in the low temperature regime, where $\lambda(T)$ is smaller than the size of a Co dot. We infer that $\lambda(0)$ in these artificially modulated superconducting films is considerably smaller than the effective penetration depth expected for a singly connected continuous thin film, in agreement with Ref. 3.

CONCLUSION

In conclusion, we have used a high-resolution scanning Hall probe microscope to identify stable vortex configurations in thin Pb films covering a square array of ferromagnetic pinning sites in a perpendicular applied field. We clearly observe that the microscopic interaction of the flux line with the local stray field favours the pinning of a flux line at that pole of the magnetic dot with the opposite sign of field. As a consequence of the broken field reversal symmetry, the pinned vortex lattices are shifted with respect to one another, depending on the field polarity. Ordered vortex structures, which are commensurate with the underlying pinning array, are observed at fields up to twice the matching field. Screening of the Co dipole fields is observed when the film is cooled below T_c in zero applied field, which we attribute to fluxoid quantization. These first local measurements indicate the subtle physics that controls the properties in these hybrid superconductor/ferromagnet structures, and further investigations will contribute to a more detailed elucidation of these pinning phenomena.

Acknowledgements

This work is supported by the Fund for Scientific Research, Flanders (FWO), the Belgian IUAP and Flemish GOA programmes, the British EPSRC and MOD grant no. GR/J03077, and the University of Bath Initiative Fund. M.J.V.B. and K.T. are Postdoctoral Research Fellows of the FWO.

REFERENCES

1. Baert M, Metlushko VV, Jonckheere R, Moshchalkov VV, Bruynseraede Y. *Phys. Rev. Lett.* 1995; **74**: 3269.
2. Moshchalkov VV, Baert M, Metlushko VV, Rosseel E, Van Bael MJ, Temst K, Jonckheere R, Bruynseraede Y. *Phys. Rev. B* 1996; **54**: 7389.
3. Moshchalkov VV, Baert M, Metlushko VV, Rosseel E, Van Bael MJ, Temst K, Jonckheere R, Bruynseraede Y. *Phys. Rev. B* 1998; **57**: 3615.
4. Harada K, Kamimura O, Kasai H, Matsuda T, Tonomura A, Moshchalkov VV. *Science* 1996; **274**: 1167.
5. Martín JI, Vélez M, Nogués J, Schuller IK. *Phys. Rev. Lett.* 1997; **79**: 1929.
6. Morgan DJ, Ketterson JB. *Phys. Rev. Lett.* 1998; **80**: 3614.
7. Van Bael MJ, Temst K, Moshchalkov VV, Bruynseraede Y. *Phys. Rev. B* 1999; **59**.
8. Lyuksyutov IF, Pokrovsky V. *Phys. Rev. Lett.* 1998; **81**: 2344.
9. Oral A, Bending SJ, Henini M. *Appl. Phys. Lett.* 1996; **69**: 1324.
10. Oral A, Barnard JC, Bending SJ, Kaya II, Ooi S, Tamegai T, Henini M. *Phys. Rev. Lett.* 1998; **80**: 3610.
11. Rosseel E, Van Bael MJ, Baert M, Jonckheere R, Moshchalkov VV, Bruynseraede Y. *Phys. Rev. B* 1996; **53**: R2983.
12. Beauchamp KM, Rosenbaum TF, Welp U, Crabtree GW, Vinokur VM. *Phys. Rev. Lett.* 1995; **75**: 3942.